

GeoMathCode: Understanding Interleaved Math-Code Reasoning for Geometry Problem Solving

Yingji Zhang^{2,3,†}, Yong Dai², André Freitas^{1,3,4}

¹ Idiap Research Institute, Switzerland, ² X-Humanoid, China

³ Department of Computer Science, University of Manchester, UK

⁴ Cancer Biomarker Centre, CRUK Manchester Institute, UK

†{firstname.lastname}3215@gmail.com

Abstract

Mathematical reasoning is a hallmark of human intelligence, requiring logical deduction, symbolic manipulation, and abstract thinking. Recent multimodal large language models (MLLMs) have demonstrated strong performance on geometry problems through multi-step reasoning. To better emulate human problem-solving, intermediate steps can incorporate auxiliary visual constructions, such as additional lines or points, which improve geometric interpretation and educational clarity. In this work, we introduce the GeoMathCode, where programmatic representations serve as intermediate visual outputs. We further conduct an in-depth analysis of the underlying reasoning geometry. Experimental results show that reasoning and code generation steps can be disentangled in the latent space, while supervised fine-tuning (SFT) makes the reasoning manifold more structured and informative. Moreover, hierarchical syntactic code structures emerge as disentangled latent subspaces, and contain more mathematical symbolic information than visual representations.

1 Introduction

Mathematical reasoning is widely regarded as a pinnacle of human intelligence, requiring a sophisticated interplay of logical deduction, symbolic manipulation, and abstract thinking. Recent advances in MLLMs have shown strong potential for mathematical reasoning (Guo et al., 2025). Given a geometry problem, MLLMs can generate multi-step solutions. To further mirror human reasoning, each step can incorporate auxiliary visual constructions, such as additional lines or points, to provide clearer geometric interpretations and enhance educational effectiveness (Shi et al., 2025).

In this scenario, traditional approaches to interleaved multimodal mathematical reasoning, such as BAGEL-Canvas (Shi et al., 2025), often rely on pixel-based image representations for auxiliary visual generation. However, this fine-grained

cross-modal generation paradigm is inherently difficult to align and verify (Chen et al., 2023) and increases system complexity by introducing additional vision-specific generator (Deng et al., 2025), increasing the potential of error propagation and inconsistency across modalities.

To address these limitations, we investigate interleaved math-code reasoning, where executable code serves as an intermediate reasoning representation for geometry problem solving, as code-based representations are inherently precise and readily verifiable. However, in this task, an important question remains unclear: *Does programmatic diagram generation fundamentally reshape the latent geometry of multimodal reasoning, or does it merely function as an auxiliary output representation?*

In particular, we seek to understand how interleaved math-code reasoning trajectories evolve across layers and reasoning steps, and whether symbolic code representations capture geometric concepts differently from visual representations.

To study these questions, we introduce a systematic pipeline for constructing a public multimodal math-code reasoning dataset, **GeoMathCode**, incorporating automated solution generation, soft rule-based evaluation, and code verification mechanisms. As illustrated in Figure 1, given a GeoMath question, we employ the representative model Gemini 3-Flash to generate interleaved math-code reasoning solutions, while GPT-5.1 is used to produce key checkpoints for textual reasoning evaluation as well as factual mathematical rules for automatic code verification. Building upon this dataset, we conduct a systematic analysis of the latent geometry underlying math-code reasoning in MLLMs from both step-wise and stage-wise perspectives, our experiments reveal several consistent findings.

Reasoning-code disentanglement. First, reasoning and code-generation steps form disentangled latent subspaces across transformer layers, suggest-

ing functional separation between mathematical reasoning and programmatic execution.

Reasoning manifold regularisation. Second, SFT regularises the latent reasoning manifold by increasing global information capacity while simultaneously reducing local geometric complexity.

Hierarchical programmatic space. Third, hierarchical programmatic syntactic structures emerge as structured latent subspaces, and latent code representations better capture fine-grained mathematical symbolic concepts than visual representations, revealing a progressive abstraction process from lexical syntax to execution-level semantics.

Overall, this work introduces a new dataset for multimodal math-code reasoning and provides insights into the latent geometric structure of reasoning processes, motivating future research on mechanistic interpretability in LLMs.

2 Related Work

In this section, we review three topics, *multimodal GeoMath datasets*, *language geometry*, and *code reasoning*, to further illustrate the motivation underlying our work.

Multimodal GeoMath Datasets. Early benchmarks such as Geometry3K (Lu et al., 2021) and ScienceQA (Lu et al., 2022) established foundational tasks for visual mathematical reasoning, while later datasets including MMMU (Yue et al., 2023), MathVista (Lu et al., 2023), MathVision (Wang et al., 2024), and MathVerse (Zhang et al., 2024a) further advanced the reasoning capabilities of multimodal models. However, most existing benchmarks focus on static problem-solution pairs and lack step-wise reasoning processes. Although MathCanvas (Shi et al., 2025) introduces interleaved visual-textual reasoning, its reliance on pixel-based visualisations complicates verification and increases system complexity. In contrast, we focus on math-code reasoning, where Python-generated geometric diagrams provide structured and verifiable visual demonstrations.

Language Geometry. The geometric structure of language representations has been extensively studied (Li et al., 2020; Chang et al., 2022; Jiang et al., 2024; Li et al., 2022; Geva et al., 2022; Nanda et al., 2023; Trager et al., 2023; Merullo et al., 2023; Turner et al., 2023). Prior work shows

that semantic representations often exhibit approximately linear structures in latent space, a phenomenon observed across modalities including vision (Huh et al., 2024), language (Trager et al., 2023), and audio (Liu et al., 2025a), and across model architectures such as Transformers (Ushio et al., 2021; Merullo et al., 2023; Hernandez et al., 2023), VAEs (Zhang et al., 2024b, 2025, 2026b; Carvalho et al., 2023), and diffusion models (Jing et al., 2022). Theoretical perspectives such as NTK-based reasoning control (Zhang et al., 2026a) and weight-space disentanglement (Ortiz-Jiménez et al., 2023) further support structured linear geometry in neural representations. Recent studies have examined geometric properties of reasoning in LLMs, including step-wise trajectories (Sun et al., 2026), layer-wise inference dynamics (Ma et al., 2026), and stage-wise training effects (Li et al., 2026; Hoogland et al., 2024). Building on these insights, we investigate the latent geometric structure underlying interleaved math-code reasoning processes.

Code Reasoning. Previous studies have shown that incorporating code during pre-training can improve agentic behaviour (Chen et al., 2025), tool use (Hong et al., 2024) and reasoning (Liu et al., 2024; Aryabumi et al., 2025), while other work reports contradictory findings on reasoning performance (Zhao et al., 2026). Other studies further explore logical reasoning through programmatic representations (Zhao et al., 2025), and Liang et al. (2025) demonstrate that grammar-based representations help LLMs distinguish subtle code differences. This work suggests that code functions primarily as an auxiliary diagram output rather than an active reasoning modality. Our experiments show that intermediate code representations do not improve textual reasoning performance and reasoning and code steps can be disentangled in the latent space, suggesting a functional separation from textual reasoning in latent space.

3 Data Construction

First, we propose an automated, verification-driven pipeline for constructing a high-quality GeoMath reasoning dataset. The pipeline is designed to ensure both the correctness and diversity of the generated samples. An overview of the overall process is illustrated in Figure 1.

To ensure comprehensive coverage of high-quality GeoMath problems, we utilise MathCanvas (Shi et al., 2025) as the primary resource, which en-

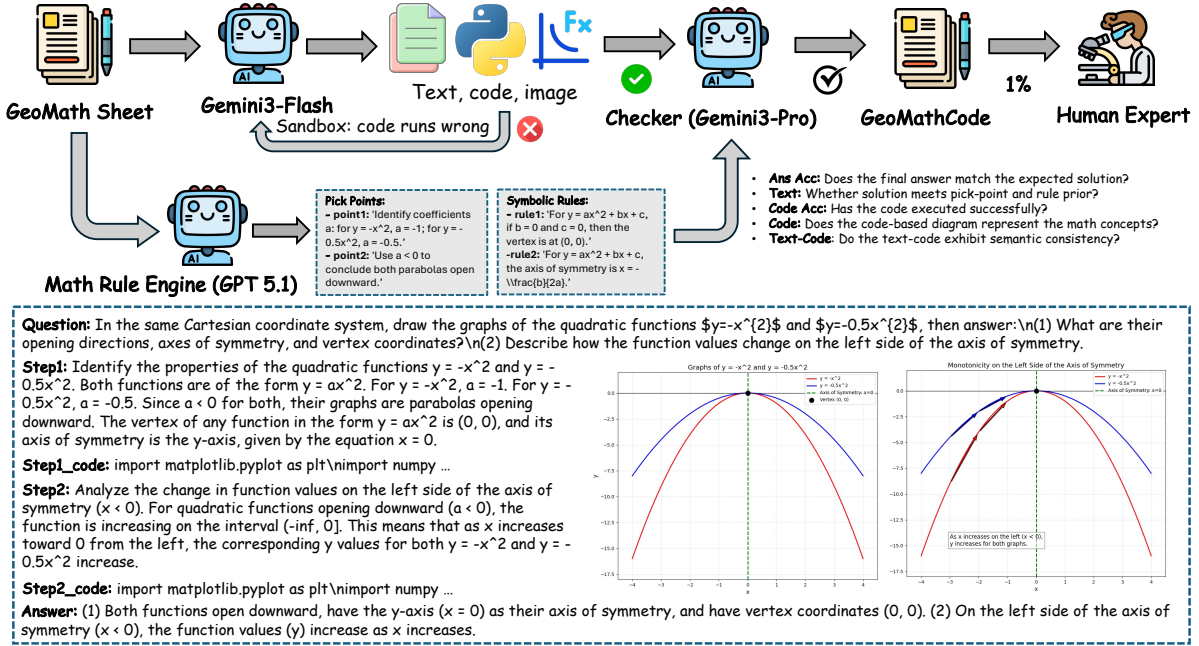


Figure 1: Pipeline overview. We construct **GeoMathCode** dataset for supervised fine-tuning.

compasses eight topics: Algebra, Analytic Geometry, Calculus, Trigonometry, Plane Geometry, Solid Geometry, Statistics, and Transformational Geometry. For each category, we first evaluate multiple state-of-the-art MLLMs as baselines (Gemini3-Flash, Gemini3-Pro, GPT-5.1, GPT-5.2) for automatic solution generation. As shown in Table 15, Gemini3 outperforms GPT5.1; therefore, we select Gemini3-Flash as the solution generator. GeoMath problems are then sourced from the dataset, and Gemini3-Flash is employed to generate solutions that integrate textual reasoning, executable Python code, and corresponding visualisations. A sandbox environment is used to ensure code validity by filtering out erroneous executions.

To enhance solution quality, we employ a rule-based engine (GPT-5.1) to extract key reasoning steps and relevant mathematical rules (Table 6) for each problem. Subsequently, an automated checker (Gemini3-Pro) performs multi-level verification, including: (i) assessing final answer correctness by comparing the outputs with reference solutions from MathCanvas, (ii) evaluating textual reasoning correctness (see prompts in Table 13), and (iii) confirming successful execution of code.

For code execution, samples that fail to execute successfully are fed back into the generator for iterative regeneration of the solution. Only samples that pass all verification stages are retained, while textual reasoning samples must achieve at least 3/5 correctness. The dataset contains multiple-choice,

fill-in-the-blank, and short-answer questions, with around 1% further reviewed by human experts. The final **GeoMathCode** dataset consists of 10k training samples and 1k test samples, balanced with a 1:1 ratio of questions with and without diagrams.

4 Empirical Analysis

In this work, we conduct experiments from two complementary perspectives: (1) post-training analysis; and (2) latent representation analysis.

4.1 Post Training Analysis

Experiment Setup. We evaluate representative models from the Qwen3/3.5 (Yang et al., 2025), LLaVA-Next (Li et al., 2024), and InternVL-3.5 (Wang et al., 2025) families. We consider both full-parameter supervised fine-tuning (SFT) and parameter-efficient tuning via LoRA (Hu et al., 2022). All models are trained in the LlamaFactory framework (Zheng et al., 2024) using a unified hyperparameter setup on 8 NVIDIA A800 GPUs. More details are provided in the Appendix A.1.

Evaluation Metrics. We evaluate reasoning capabilities using five metrics: (1) *Ans Acc*: final answer accuracy; (2) *Text*: correctness of the textual reasoning, measured as the average of the point selection score and rule application score; (3) *Code Acc*: accuracy of the executable Python code; (4) *Code*: mathematical correctness of the generated code; and (5) *Text-Code*: consistency between the

MLLM	Opt.	Ans Acc	Text	Code Acc	Code	Text Code	Avg.
Qwen3-VL-Ins-8B	-	0.32	0.38	0.59	0.41	0.37	0.41
Qwen3-VL-Ins-8B	SFT	0.48	0.57	0.97	0.70	0.68	0.71
Qwen3-VL-Think-8B	SFT	0.44	0.50	0.86	0.69	0.59	0.62
Qwen3-VL-Ins-8B	LoRA	0.41	0.51	0.85	0.68	0.57	0.60
Qwen3.5-4B	SFT	0.42	0.51	0.93	0.73	0.60	0.64
Qwen3.5-9B	SFT	0.55	0.65	0.97	0.76	0.73	0.73
Qwen3.5-9B	LoRA	0.54	0.64	0.94	0.80	0.70	0.72
LLaVA-NEXT-8B	-	0.00	0.00	0.00	0.00	0.00	0.00
LLaVA-NEXT-8B	SFT	0.15	0.23	0.83	0.43	0.26	0.38
InternVL3.5-8B	-	0.29	0.33	0.53	0.57	0.47	0.44
InternVL3.5-8B	SFT	0.48	0.58	0.96	0.70	0.68	0.68

Table 1: Comparison of the performance of open-source MLLMs on the **GeoMathCode** dataset, evaluated using Gemini3-Pro due to its higher Spearman correlation between *Ans Acc* and *Text* scores. More experimental details are provided in Appendix A.3.

MLLM	Ans Acc-Text	Ans Acc-Text Code	Ans Acc-Code
<i>without rule instruction</i>			
Qwen3-VL-Ins-8B-SFT	0.48	0.48	0.22
Qwen3.5-9B-SFT	0.49	0.47	0.21
Qwen3.5-9B-LoRA	0.50	0.47	0.22
InternVL3.5-8B-SFT	0.48	0.47	0.23
<i>with rule instruction</i>			
Qwen3-VL-Ins-8B-SFT	0.70	0.70	0.23
Qwen3.5-9B-SFT	0.69	0.70	0.20
Qwen3.5-9B-LoRA	0.70	0.70	0.23
InternVL3.5-8B-SFT	0.71	0.70	0.23

Table 2: Pearson (left) and Spearman (right) correlation between different metrics. Same observation when using GPT5.1 and DeepSeek-V4-Flash as LLM evaluators in Table 16 and 17, respectively.

Evaluator 1	Evaluator 2	Ans Acc	Text	Code	Text Code
Gemini3-Pro	GPT-5.1	0.96	0.69	0.57	0.50
Gemini3-Pro	DeepSeek-V4-Flash	0.99	0.94	0.70	0.70
GPT-5.1	DeepSeek-V4-Flash	0.96	0.68	0.58	0.54

Table 3: Spearman correlation between different LLM evaluators on the prediction of Qwen3.5-9B-SFT.

textual reasoning step and the corresponding code.

For *Ans Acc*, a mixed evaluation strategy is adopted: multiple-choice and numerical fill-in-the-blank questions are evaluated using exact match, while all other question types are assessed by MLLM evaluators. Metrics 1, 2, 4, and 5 are then computed using the scores from Gemini3-Pro as we find that the Gemini3-Pro has the higher Spearman correlation between *Ans Acc* and *Text* than GPT-5.1 and DeepSeek-V4-Flash. Finally, all scores are normalised to the range (0, 1). More details are

provided in Appendix A.3.

As shown in Table 1, after the SFT stage, Qwen3.5 consistently outperforms all baseline models. Among them, Qwen3.5-9B achieves the best overall performance, followed by the LoRA-based setup, demonstrating the strong capability of the base model on this downstream task.

(1) Point- and rule-based instructions during evaluation improve the Text-Ans Acc alignment. Furthermore, we examine the relationships among evaluation metrics by computing both Pearson and

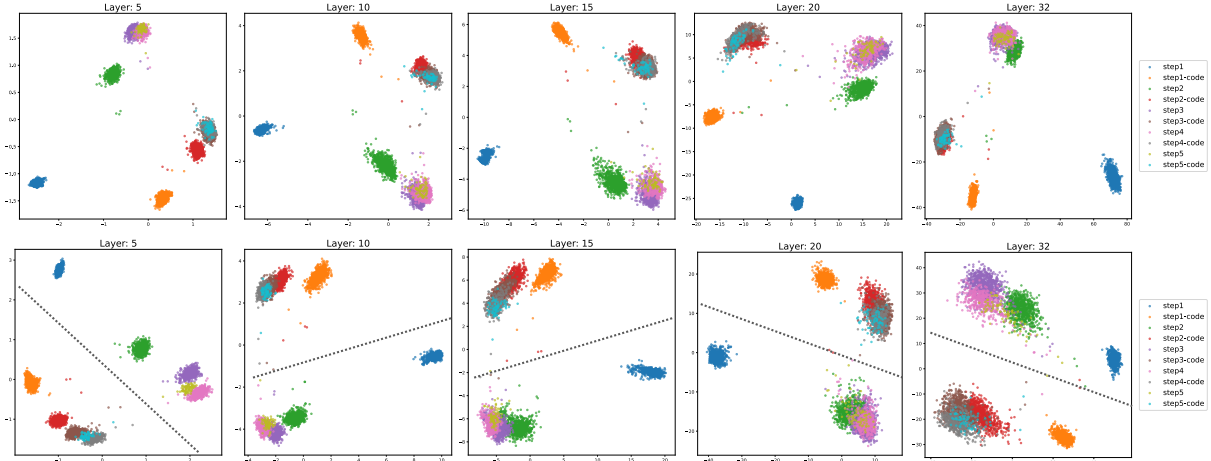


Figure 2: PCA visualisation of the reasoning step and code step geometry (Top: Qwen3.5-9B, bottom: Qwen3.5-9B-SFT). We can observe that reasoning and code steps can be disentangled in the latent space.

Spearman correlation coefficients. As reported in Table 2, incorporating pick-point-based instructions during evaluation improves the alignment between textual reasoning quality and final answer accuracy (Ans-Text). This finding suggests that such constraints enable the LLM evaluator to produce more consistent judgments, indicating a positive correlation between the logical coherence of reasoning process and the correctness of the final generated answer. More importantly, this observation highlights the potential of using intermediate pick-point and rule-based supervision signals for multi-step reinforcement learning.

Conversely, this incorporation does not improve the alignment between final-answer accuracy and text-code or Code, suggesting that intermediate code representations contribute less directly to final-answer prediction. This further indicates a potential functional disentanglement between reasoning and coding processes in the latent space, motivating our subsequent investigation of latent geometry.

4.2 Reasoning Geometry Analysis

4.2.1 Reasoning Trajectory

First, we analyse the overall geometry of multi-step reasoning in the latent space of MLLM.

Experiment Setup. Prior studies have shown that reasoning-step markers contain informative geometric structures associated with reasoning trajectories (Sun et al., 2026). Therefore, for each question in the test set, we generate the multi-step reasoning solution via greedy search and extract hidden representations of the token corresponding to the *step* and *step_code* marker, denoted

as $\mathbf{h}_t^{(\ell)}(\text{step}_k)$ and $\mathbf{h}_t^{(\ell)}(\text{step}_k\text{-code})$, which captures the model’s initial information transitioning to the reasoning step. The ordered sequence $\mathbf{h}_t^{(\ell)}(\text{step}_1)$, $\mathbf{h}_t^{(\ell)}(\text{step}_1\text{-code})$, \dots , $\mathbf{h}_t^{(\ell)}(\text{step}_N)$, and $\mathbf{h}_t^{(\ell)}(\text{step}_N\text{-code})$ thus provides a series of reasoning trajectory of the model’s internal representations.

(1) Reasoning and code steps are geometrically separable in the latent space. Figure 2 shows clear separability across reasoning stages and between reasoning and code representations. Notably, Step 1 forms a geometrically isolated region across layers, suggesting its role in semantic grounding and problem initialisation, while later reasoning steps progressively converge into a shared reasoning manifold.

MLLM	Ans Acc	Text	Avg.
<i>with code</i>			
Qwen3-VL-Ins-8B	0.32	0.38	0.35
Qwen3-VL-Ins-8B-SFT	0.48	0.57	0.53
Qwen3.5-9B-SFT	0.55	0.65	0.60
<i>without code</i>			
Qwen3-VL-Ins-8B	0.33	0.38	0.36
Qwen3-VL-Ins-8B-SFT	0.48	0.57	0.53
Qwen3.5-9B-SFT	0.54	0.65	0.60

Table 4: Performance of GeoMathCode without code generation.

In addition to PCA, we also compared with Qwen3 and 3.5 with or without code generation setup to further evaluate the separation between text and code reasoning. As shown in Table 4, both settings achieve highly similar performance, suggesting a functional separation between textual

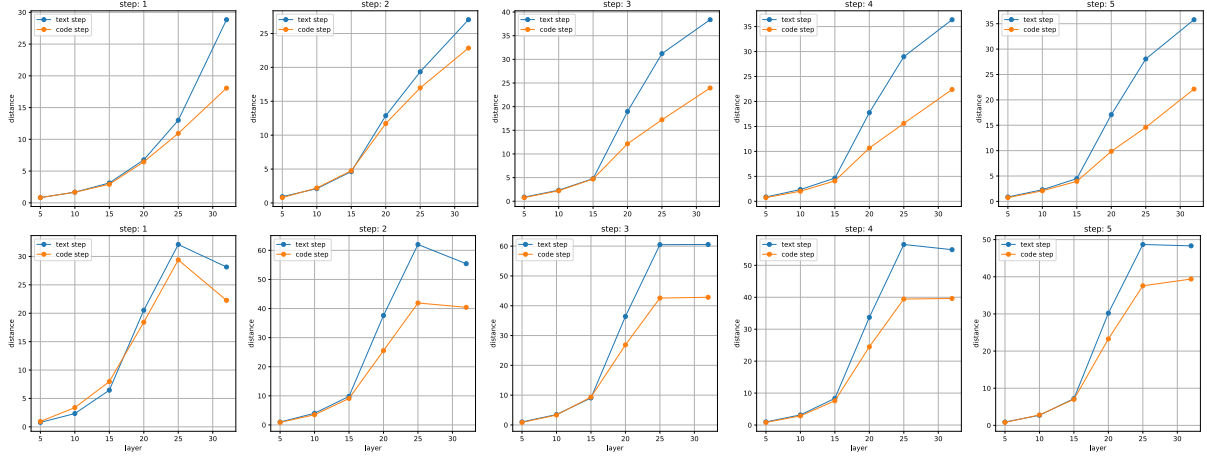


Figure 3: Average euclidean distance of different steps at different layers (Top: Qwen3.5-9B, bottom: Qwen3.5-9B-SFT). Same observation for Qwen3-VL-8B and InternVL3.5-8B in Figure 6 and 7.

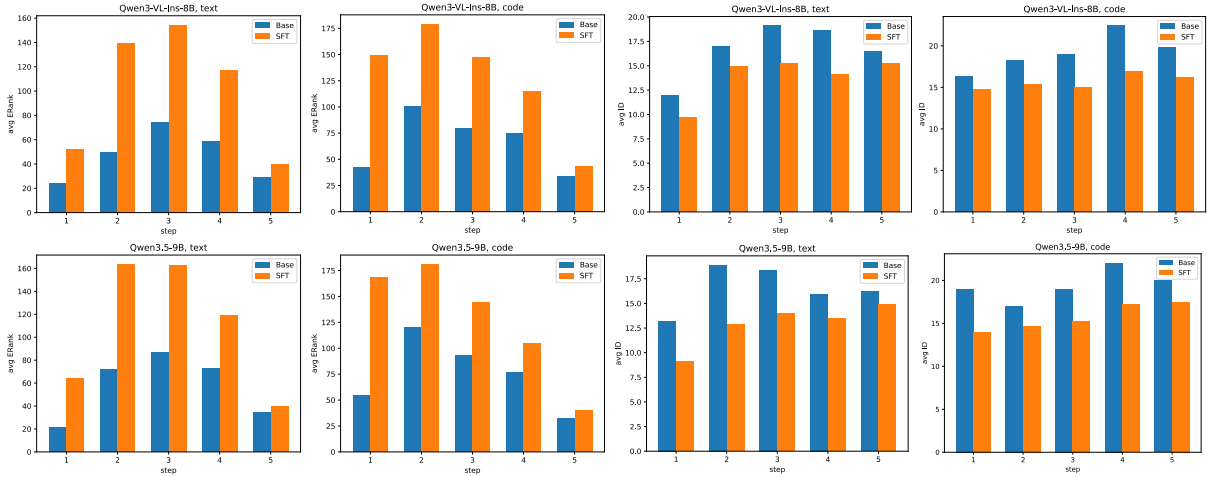


Figure 4: ERank \uparrow (left) and ID \downarrow (right) for Qwen3-VL-Ins-8B (top) and Qwen3.5-9B (bottom).

reasoning and diagram generation. Specifically, the model primarily relies on textual reasoning trajectories for final-answer prediction, while intermediate code generation mainly serves as an auxiliary executable representation rather than an active reasoning modality. This behaviour differs from visual interleaved chain-of-thought settings, where visual modalities can directly contribute to and guide the reasoning process (Hu et al., 2024; Deng et al., 2025; Liu et al., 2025b). Instead, these findings align with recent studies showing that programmatic data do not necessarily provide additive improvements to model capabilities in complex math reasoning task (Zhao et al., 2026).

(2) Deep layers exhibit a more diverse reasoning regime. To better understand the reasoning step geometry, we measure the average euclidean distance between central point and others within each reasoning step cluster. As illustrated in Fig-

ure 3, we observe that the intra-step representation distance progressively increases with layer depth, suggesting that the model enters a more diverse and computation-dependent reasoning regime during later layers of problem solving. The comparatively smaller distances observed in code reasoning further suggest that program-based reasoning follows a more constrained and structurally regular latent trajectory than free-form textual reasoning.

(3) SFT makes reasoning steps manifold more informative and regular. Interestingly, we can observe that SFT stage simultaneously increases the intra-step representation distance. This suggests that SFT does not merely compress reasoning representations into more compact manifolds, but instead promotes richer intermediate reasoning information. To quantify the information capacity and geometric complexity of reasoning representations, we measure both the *Effective Rank (ERank)*

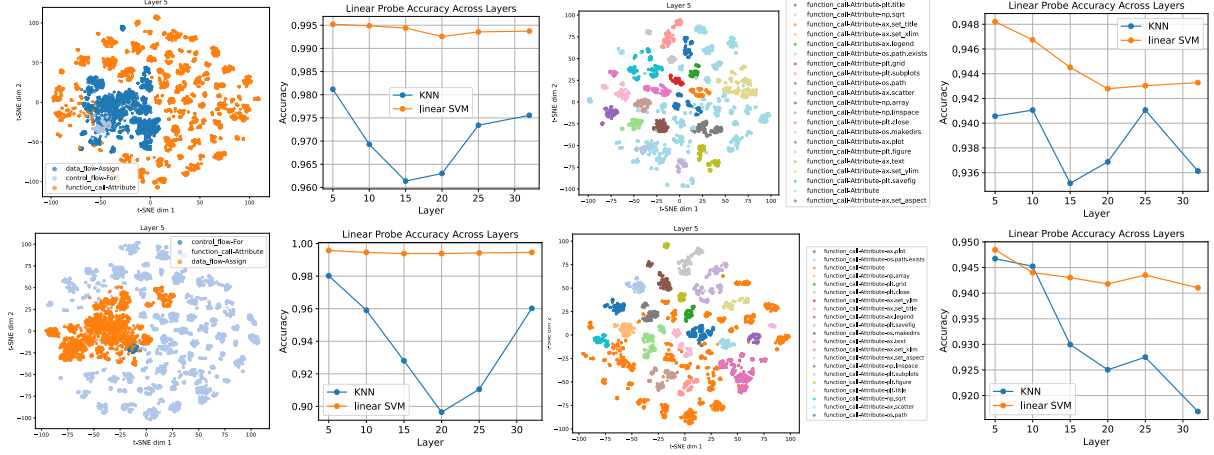


Figure 5: Code syntax space visualisation and linear probing results for Qwen3.5-9B (Top) and Qwen3.5-9B-SFT (Bottom). Left: visualisation of the representation spaces corresponding to high-level program semantics: control_flow, function_call, and data_flow; right: fine-grained analysis of the function_call category.

and the *Intrinsic Dimensionality (ID)* of hidden states across different layers and reasoning steps. Given the covariance matrix Σ of hidden representations, let $\{\lambda_i\}_{i=1}^d$ denote its eigenvalue spectrum and define the normalised spectrum as $p_i = \frac{\lambda_i}{\sum_{j=1}^d \lambda_j}$. The *Effective Rank (ERank)* is defined as the exponential of the spectral entropy: $\text{ERank}(\Sigma) = \exp\left(-\sum_{i=1}^d p_i \log p_i\right)$, which characterises how evenly information spreads across eigen-directions. A larger ERank indicates that the representation manifold spreads across more informative directions, reflecting richer and more diverse latent patterns. For the *Intrinsic Dimensionality (ID)*, it is defined as $\text{ID}(\Sigma) = \frac{(\sum_{i=1}^d \lambda_i)^2}{\sum_{i=1}^d \lambda_i^2}$. It measures the number of dominant dimensions contributing to the representation space (i.e., local manifold complexity). Higher ID corresponds to more complex local geometry, while lower ID indicates more regular and constrained representation structures.

As shown in Figure 4, SFT increases the ERank of reasoning representations while reducing their ID, suggesting a more informative yet geometrically regular reasoning manifold. This suggests that SFT does not simply increase representational complexity in an unconstrained manner, but instead promotes a more structured organisation of the latent reasoning manifold, reflecting increasingly constrained and canonical reasoning trajectories after fine-tuning.

This observation provides several important insights. First, stronger reasoning representations are not necessarily associated with higher geometric complexity. Instead, effective reasoning appears

to require a balance between information diversity and geometric regularity. Second, rather than compressing representations into smaller latent regions, SFT reorganises reasoning trajectories into more canonical and reusable computational paths, which provides a strong motivation for future study in intermediate supervision in reasoning training.

4.2.2 Geometrical Structure of Code Space

Next, we focus on the geometric structure of code space, as it follows structured and deterministic processes. Studying code space therefore provides clearer insights into the syntactic and semantic structures encoded in latent representations.

Experiment Setup. In the experiment, we extract the generated code at the middle reasoning step and employ Abstract Syntax Tree (AST) parser to automatically identify the structure information (e.g., function call, data structure, etc.) and extract the corresponding hidden representations.

First, we analyse high-level syntax categories, including control flow (e.g., for loop), function calls (e.g., np.array), and data flow (e.g., variable assignments), as well as the fine-grained structure within the *function call* category. We use KNN and linear SVM to evaluate the local structure and global linear separability, respectively.

(1) Hierarchical syntactic code structures can be disentangled and represented as latent subspaces.

As illustrated in Figure 5 (t-SNE visualisation), distinct fine-grained programmatic syntactic structures (e.g., function_call) can be separated in the latent space, suggesting that the model organises different code semantics into structured rep-

representation subspaces. Meanwhile, certain high-level structures display partial overlap due to their compositional nature. For example, for loops are not purely control-flow operations, but also implicitly involve variable assignment, iteration-state updates, and function-call semantics. Consequently, their representations partially overlap with both `data_flow` and `function_call` subspaces, indicating that intermediate code representations encode compositional execution semantics rather than isolated syntactic categories alone.

(2) Latent code representations progressively lose locally compact lexical clustering while preserving globally linearly semantic structures. Next, as shown in Figure 5 (accuracy curve), we can observe that SVM has a higher accuracy than KNN, a higher linear SVM accuracy indicates that information remains globally linear in the latent space. In other words, the model has not completely discarded specific information, e.g., different function calls can still be separated by global semantic directions. In contrast, the decline in KNN accuracy suggests that local neighborhood structures become increasingly mixed in deeper layers. Function calls with similar computational roles, such as plotting- or rendering-related APIs, begin to overlap within local regions of the latent space. This indicates that the model no longer represents APIs as isolated lexical categories, but instead reorganises them into shared execution-semantic manifolds based on their functional roles in program execution.

The results reveal a potential hierarchical abstraction dynamic in code representations. High-level semantic abstractions, such as control-flow, data-flow, and function-call categories, remain relatively preserved throughout layer evolution, while fine-grained lexical and syntactic information becomes dynamically entangled or separated across layers.

These findings may inspire future studies on the mechanisms of function-calling and executable reasoning in LLMs, where latent code-generation states may resemble structured state-transition processes similar to state machines. Mechanistic interpretability approaches, such as sparse autoencoders and circuit analysis, may further help uncover the internal computational structures underlying these executable reasoning behaviours.

(3) Latent code representations better capture fine-grained mathematical symbolic concepts than visual representations. Finally, we evalu-

ate whether code representations preserve more fine-grained mathematical symbolic information than visual representations. For each mathematical question, we assign labels based on the exact occurrence of specific symbolic categories, including `frac`, `sqrt`, `circ`, `triangle`, `angle`, `begincases`, `sin`, and `overrightarrow`, within mathematical formulas delimited by ($\$formula\$$). Each symbolic corresponds to distinct metathetical concept.

We then extract the corresponding pooled code representations and rendered visual representations by feeding them into an MLLM encoder. A classifier is subsequently trained to evaluate the representational capabilities of each modality. As reported in Table 5, code representations achieve higher accuracy, indicating that latent code embeddings capture fine-grained mathematical symbolic concepts more effectively than visual representations. Furthermore, compared to the base model, SFT enhances the model’s ability to represent fine-grained mathematical expressions.

classifier	Code	Image	Code	Image
<i>Layer 10</i>				
KNN	0.66	0.65	0.67	0.65
SVM	0.82	0.77	0.83	0.77
RF	0.69	0.67	0.71	0.66
<i>Layer 20</i>				
KNN	0.66	0.63	0.70	0.67
SVM	0.81	0.76	0.83	0.78
RF	0.70	0.66	0.72	0.66
<i>Layer 32</i>				
KNN	0.66	0.65	0.66	0.65
SVM	0.83	0.75	0.84	0.75
RF	0.70	0.69	0.71	0.65

Table 5: Fine-grained probing on math symbolic concepts (left: Qwen3.5-9B, right: Qwen3.5-9B-SFT), where RF is random forest.

5 Conclusion

In this work, we introduce the GeoMathCode dataset, where programmatic representations serve as intermediate visual outputs. We further conduct an in-depth analysis of the underlying reasoning process. Experimental results show that reasoning and code generation steps can be disentangled in the latent space, while SFT makes the reasoning manifold more structured and informative. Moreover, hierarchical syntactic code structures emerge as disentangled latent subspaces, suggesting a hierarchical abstraction process during reasoning. These findings can inspire our future studies on the mechanistic interpretability of code execution, pick-point-based reinforcement learning, etc.

Limitations

This work has several limitations. First, the automatic evaluation pipeline relies heavily on MLLM-based judgment, which may introduce biases and inconsistencies in assessing reasoning quality. Although point- and rule-based instructions improve evaluation alignment, the reliability and robustness of LLM evaluators remain limited compared to human expert annotation. In particular, the evaluator may fail to accurately distinguish subtle logical errors or overestimate superficially coherent reasoning traces. Second, the overall final answer accuracy remains relatively low. This suggests that improvements in reasoning capability and final answer prediction are still necessary. To address these limitations, future work will focus on developing automatic symbolic evaluation methods for multi-step reasoning processes and exploring reinforcement learning approaches, such as GRPO (Shao et al., 2024) and DAPO (Yu et al., 2026), to further improve final answer accuracy and reasoning reliability.

References

- Viraat Aryabumi, Yixuan Su, Raymond Ma, Adrien Morisot, Ivan Zhang, Acyr Locatelli, Marzieh Fadaee, Ahmet Üstün, and Sara Hooker. 2025. To code or not to code? exploring impact of code in pre-training. In *International Conference on Learning Representations*, volume 2025, pages 79469–79495.
- Danilo S. Carvalho, Yingji Zhang, Giangiacomo Mercatali, and Andre Freitas. 2023. Learning disentangled representations for natural language definitions. *Findings of the European chapter of Association for Computational Linguistics (Findings of EACL)*.
- Tyler A Chang, Zhuowen Tu, and Benjamin K Bergen. 2022. The geometry of multilingual language model representations. *arXiv preprint arXiv:2205.10964*.
- Gongwei Chen, Leyang Shen, Rui Shao, Xiang Deng, and Liqiang Nie. 2023. **Lion : Empowering multimodal large language model with dual-level visual knowledge**. *2024 IEEE/CVF Conference on Computer Vision and Pattern Recognition (CVPR)*, pages 26530–26540.
- Kevin Chen, Marco Cusumano-Towner, Brody Hual, Aleksei Petrenko, Jackson Hamburger, Vladlen Koltun, and Philipp Krähenbühl. 2025. Reinforcement learning for long-horizon interactive llm agents. *arXiv preprint arXiv:2502.01600*.
- Chaorui Deng, Deyao Zhu, Kunchang Li, Chenhui Gou, Feng Li, Zeyu Wang, Shu Zhong, Weihao Yu, Xiaonan Nie, Ziang Song, et al. 2025. Emerging properties in unified multimodal pretraining. *arXiv preprint arXiv:2505.14683*.
- Mor Geva, Avi Caciularu, Kevin Ro Wang, and Yoav Goldberg. 2022. Transformer feed-forward layers build predictions by promoting concepts in the vocabulary space. *arXiv preprint arXiv:2203.14680*.
- Daya Guo, Dejian Yang, Haowei Zhang, Junxiao Song, Peiyi Wang, Qihao Zhu, Runxin Xu, Ruoyu Zhang, Shirong Ma, Xiao Bi, et al. 2025. Deepseek-r1: Incentivizing reasoning capability in llms via reinforcement learning. *arXiv preprint arXiv:2501.12948*.
- Evan Hernandez, Arnab Sen Sharma, Tal Haklay, Kevin Meng, Martin Wattenberg, Jacob Andreas, Yonatan Belinkov, and David Bau. 2023. Linearity of relation decoding in transformer language models. *arXiv preprint arXiv:2308.09124*.
- Sirui Hong, Mingchen Zhuge, Jonathan Chen, Xiawu Zheng, Yuheng Cheng, Jinlin Wang, Ceyao Zhang, Steven Yau, Zijuan Lin, Liyang Zhou, et al. 2024. Metagpt: Meta programming for a multi-agent collaborative framework. In *International Conference on Learning Representations*, volume 2024, pages 23247–23275.
- Jesse Hoogland, George Wang, Matthew Farrugia-Roberts, Liam Carroll, Susan Wei, and Daniel Murefet. 2024. Loss landscape degeneracy and stage-wise development in transformers. *arXiv preprint arXiv:2402.02364*.
- Edward J Hu, Yelong Shen, Phillip Wallis, Zeyuan Allen-Zhu, Yuanzhi Li, Shean Wang, Liang Wang, Weizhu Chen, et al. 2022. Lora: Low-rank adaptation of large language models. *Iclr*, 1(2):3.
- Yushi Hu, Weijia Shi, Xingyu Fu, Dan Roth, Mari Ostendorf, Luke Zettlemoyer, Noah A Smith, and Ranjay Krishna. 2024. Visual sketchpad: Sketching as a visual chain of thought for multimodal language models. *Advances in Neural Information Processing Systems*, 37:139348–139379.
- Minyoung Huh, Brian Cheung, Tongzhou Wang, and Phillip Isola. 2024. The platonic representation hypothesis. *arXiv preprint arXiv:2405.07987*.
- Yibo Jiang, Bryon Aragam, and Victor Veitch. 2024. Uncovering meanings of embeddings via partial orthogonality. *Advances in Neural Information Processing Systems*, 36.
- Bowen Jing, Gabriele Corso, Renato Berlinghieri, and Tommi Jaakkola. 2022. Subspace diffusion generative models. In *European conference on computer vision*, pages 274–289. Springer.
- Bohan Li, Hao Zhou, Junxian He, Mingxuan Wang, Yiming Yang, and Lei Li. 2020. On the sentence embeddings from pre-trained language models. *arXiv preprint arXiv:2011.05864*.

- Feng Li, Renrui Zhang, Hao Zhang, Yuanhan Zhang, Bo Li, Wei Li, Zejun Ma, and Chunyuan Li. 2024. Llava-next-interleave: Tackling multi-image, video, and 3d in large multimodal models. *arXiv preprint arXiv:2407.07895*.
- Kenneth Li, Aspen K Hopkins, David Bau, Fernanda Viégas, Hanspeter Pfister, and Martin Wattenberg. 2022. Emergent world representations: Exploring a sequence model trained on a synthetic task. *arXiv preprint arXiv:2210.13382*.
- Melody Li, Kumar Krishna Agrawal, Arna Ghosh, Komal Teru, Adam Santoro, Guillaume Lajoie, and Blake Richards. 2026. Tracing the representation geometry of language models from pretraining to post-training. *Advances in Neural Information Processing Systems*, 38:54691–54724.
- Qingyuan Liang, Zhao Zhang, Zeyu Sun, Zheng Lin, Qi Luo, Yueyi Xiao, Yizhou Chen, Yuqun Zhang, Haotian Zhang, Lu Zhang, Bin Chen, and Yingfei Xiong. 2025. Grammar-based code representation: Is it a worthy pursuit for LLMs? In *Findings of the Association for Computational Linguistics: ACL 2025*, pages 15640–15653, Vienna, Austria. Association for Computational Linguistics.
- Che Liu, Yingji Zhang, Dong Zhang, Weijie Zhang, Chenggong Gong, Yu Lu, Shilin Zhou, Ziliang Gan, Ziao Wang, Haipang Wu, et al. 2025a. Nexus-o: An omni-perceptive and-interactive model for language, audio, and vision. In *Proceedings of the 33rd ACM International Conference on Multimedia*, pages 10787–10796.
- Dairu Liu, Ziyue Wang, Minyuan Ruan, Fuwen Luo, Chi Chen, Peng Li, and Yang Liu. 2025b. Thinking with visual abstract: Enhancing multimodal reasoning via visual abstraction. *arXiv preprint arXiv:2505.20164*.
- Yue Liu, Yue Yu, Yuanliang Zhang, Yu Jiang, Changjian Wang, Shanshan Li, et al. 2024. At which training stage does code data help llms reasoning? In *International Conference on Learning Representations*, volume 2024, pages 36281–36300.
- Pan Lu, Hritik Bansal, Tony Xia, Jiacheng Liu, Chunyue Li, Hannaneh Hajishirzi, Hao Cheng, Kai-Wei Chang, Michel Galley, and Jianfeng Gao. 2023. Mathvista: Evaluating mathematical reasoning of foundation models in visual contexts. In *International Conference on Learning Representations*.
- Pan Lu, Ran Gong, Shibiao Jiang, Liang Qiu, Siyuan Huang, Xiaodan Liang, and Song-Chun Zhu. 2021. Inter-gps: Interpretable geometry problem solving with formal language and symbolic reasoning. In *Annual Meeting of the Association for Computational Linguistics*.
- Pan Lu, Swaroop Mishra, Tony Xia, Liang Qiu, Kai-Wei Chang, Song-Chun Zhu, Oyvind Tafjord, Peter Clark, and A. Kalyan. 2022. Learn to explain: Multimodal reasoning via thought chains for science question answering. *ArXiv*, abs/2209.09513.
- Yanbiao Ma, Fei Luo, Linfeng Zhang, Chuangxin Zhao, Mingxuan Wang, Yinan Wu, Zhe Qian, Yang Lu, Long Chen, Zhao Cao, Xiaoshuai Hao, Ji-Rong Wen, and Jungong Han. 2026. Reasoning emerges from constrained inference manifolds in large language models.
- Jack Merullo, Carsten Eickhoff, and Ellie Pavlick. 2023. Language models implement simple word2vec-style vector arithmetic. *arXiv preprint arXiv:2305.16130*.
- Neel Nanda, Andrew Lee, and Martin Wattenberg. 2023. Emergent linear representations in world models of self-supervised sequence models. *arXiv preprint arXiv:2309.00941*.
- Guillermo Ortiz-Jiménez, Alessandro Favero, and Pascal Frossard. 2023. Task arithmetic in the tangent space: Improved editing of pre-trained models. *ArXiv*, abs/2305.12827.
- Zhihong Shao, Peiyi Wang, Qihao Zhu, Runxin Xu, Junxiao Song, Xiao Bi, Haowei Zhang, Mingchuan Zhang, YK Li, Yang Wu, et al. 2024. Deepseekmath: Pushing the limits of mathematical reasoning in open language models. *arXiv preprint arXiv:2402.03300*.
- Weikang Shi, Aldrich Yu, Rongyao Fang, Houxing Ren, Ke Wang, Aojun Zhou, Changyao Tian, Xinyu Fu, Yuxuan Hu, Zimu Lu, et al. 2025. Mathcanvas: Intrinsic visual chain-of-thought for multimodal mathematical reasoning. *arXiv preprint arXiv:2510.14958*.
- Lihao Sun, Hang Dong, Bo Qiao, Qingwei Lin, Dongmei Zhang, and S. Rajmohan. 2026. Llm reasoning as trajectories: Step-specific representation geometry and correctness signals.
- Matthew Trager, Pramuditha Perera, Luca Zancato, Alessandro Achille, Parminder Bhatia, and Stefano Soatto. 2023. Linear spaces of meanings: compositional structures in vision-language models. In *Proceedings of the IEEE/CVF International Conference on Computer Vision*, pages 15395–15404.
- Alex Turner, Lisa Thiergart, David Udell, Gavin Leech, Ulisse Mini, and Monte MacDiarmid. 2023. Activation addition: Steering language models without optimization. *arXiv preprint arXiv:2308.10248*.
- Asahi Ushio, Luis Espinosa-Anke, Steven Schockaert, and Jose Camacho-Collados. 2021. Bert is to nlp what alexnet is to cv: Can pre-trained language models identify analogies? *arXiv preprint arXiv:2105.04949*.
- Ke Wang, Junting Pan, Weikang Shi, Zimu Lu, Houxing Ren, Aojun Zhou, Mingjie Zhan, and Hongsheng Li. 2024. Measuring multimodal mathematical reasoning with MATH-vision dataset. In *The Thirty-eight Conference on Neural Information Processing Systems Datasets and Benchmarks Track*.

Weiyun Wang, Zhangwei Gao, Lixin Gu, Hengjun Pu, Long Cui, Xingguang Wei, Zhaoyang Liu, Linglin Jing, Shenglong Ye, Jie Shao, et al. 2025. Internvl3.5: Advancing open-source multimodal models in versatility, reasoning, and efficiency. *arXiv preprint arXiv:2508.18265*.

An Yang, Anfeng Li, Baosong Yang, Beichen Zhang, Binyuan Hui, Bo Zheng, Bowen Yu, Chang Gao, Chengen Huang, Chenxu Lv, et al. 2025. Qwen3 technical report. *arXiv preprint arXiv:2505.09388*.

Qiyang Yu, Zheng Zhang, Ruofei Zhu, Yufeng Yuan, Xiaochen Zuo, Yu Yue, Weinan Dai, Tiantian Fan, Gaohong Liu, Lingjun Liu, et al. 2026. Dapo: An open-source llm reinforcement learning system at scale. *Advances in Neural Information Processing Systems*, 38:113222–113244.

Xiang Yue, Yuansheng Ni, Kai Zhang, Tianyu Zheng, Ruoqi Liu, Ge Zhang, Samuel Stevens, Dongfu Jiang, Weiming Ren, Yuxuan Sun, Cong Wei, Botao Yu, Ruibin Yuan, Renliang Sun, Ming Yin, Boyuan Zheng, Zhenzhu Yang, Yibo Liu, Wenhao Huang, Huan Sun, Yu Su, and Wenhao Chen. 2023. *Mmmu: A massive multi-discipline multimodal understanding and reasoning benchmark for expert agi*. 2024 *IEEE/CVF Conference on Computer Vision and Pattern Recognition (CVPR)*, pages 9556–9567.

Renrui Zhang, Xinyu Wei, Dongzhi Jiang, Ziyu Guo, Shicheng Li, Yichi Zhang, Chengzhuo Tong, Jiaming Liu, Aojun Zhou, Bin Wei, Shanghang Zhang, Peng Gao, Chunyuan Li, and Hongsheng Li. 2024a. *Mavis: Mathematical visual instruction tuning with an automatic data engine*.

Yingji Zhang, Danilo Carvalho, and Andre Freitas. 2024b. *Learning disentangled semantic spaces of explanations via invertible neural networks*. In *Proceedings of the 62nd Annual Meeting of the Association for Computational Linguistics (Volume 1: Long Papers)*, pages 2113–2134, Bangkok, Thailand. Association for Computational Linguistics.

Yingji Zhang, Danilo Carvalho, and Andre Freitas. 2025. *Quasi-symbolic semantic geometry over transformer-based variational AutoEncoder*. In *Proceedings of the 29th Conference on Computational Natural Language Learning*, pages 12–29, Vienna, Austria. Association for Computational Linguistics.

Yingji Zhang, Danilo Carvalho, and Andre Freitas. 2026a. *Guiding explanatory inference through inference types*.

Yingji Zhang, Marco Valentino, Danilo Carvalho, and André Freitas. 2026b. *Learning to disentangle latent reasoning rules with language vaes: a systematic study*. In *Proceedings of the AAAI Conference on Artificial Intelligence*, volume 40, pages 19458–19466.

Yuze Zhao, Junpeng Fang, Lu Yu, Zhenya Huang, Kai Zhang, Qing Cui, Qi Liu, Jun Zhou, and Enhong Chen. 2026. *What really improves mathematical*

reasoning: Structured reasoning signals beyond pure code. *arXiv preprint arXiv:2605.19762*.

Yuze Zhao, Tianyun Ji, Wenjun Feng, Zhenya Huang, Qi Liu, Zhiding Liu, Yixiao Ma, Kai Zhang, and Enhong Chen. 2025. *Unveiling the magic of code reasoning through hypothesis decomposition and amendment*. In *The Thirteenth International Conference on Learning Representations*.

Yaowei Zheng, Richong Zhang, Junhao Zhang, Yanhan Ye, Zheyang Luo, Zhangchi Feng, and Yongqiang Ma. 2024. *Llamafactory: Unified efficient fine-tuning of 100+ language models*. In *Proceedings of the 62nd Annual Meeting of the Association for Computational Linguistics (Volume 3: System Demonstrations)*, Bangkok, Thailand. Association for Computational Linguistics.

A Appendix

A.1 Experiment Details

GeoMathCode Dataset. After tokenisation and applying the chat template, the average sequence length of GeoMathCode is 3020 tokens. In terms of reasoning depth (measured on the training set), 9683 samples has three steps, 5717 samples contain four reasoning steps, 946 samples contain five reasoning steps, and 67 samples contain six reasoning steps, indicating that the dataset predominantly consists of long-form multi-step reasoning trajectories. Table 7 and Table 6 present representative examples of extracted pick-points and symbolic mathematical rules used in the automatic verification pipeline.

Atomic Rules:

1. Perimeter($\triangle ABC$) = $AB + BC + CA$.
2. $r = d/2$
3. A linear pair of adjacent angles forms a straight angle: $m\angle 1 + m\angle 2 = 180^\circ$.

Conditional Rules:

1. Definition of midpoint: If M is midpoint of segment PQ , then $PM = MQ$ and M lies on PQ .
2. All radii of a circle are equal: if O is the center, then $OA = OB = OC = r$.
3. If all three sides of a triangle are equal, then the triangle is equilateral.

Table 6: Example of math rules for plane geometry category.

Training Setups. For full-parameter SFT, model is trained using DeepSpeed ZeRO-3 optimisation with a per-device batch size of 1 and gradient accumulation over 8 steps. For LoRA-based training, LoRA adapters are applied to all trainable modules

1. Recognizes both functions are of the form $y = ax^2$ with $a = -1$ and $a = -0.5$.
2. Uses $a < 0$ to conclude both parabolas open downward.
3. Identifies vertex at $(0, 0)$ for functions of the form $y = ax^2$ with no linear or constant term.
4. Identifies axis of symmetry as $x = 0$ (the y-axis).
5. States that for a downward-opening parabola, the function is increasing on $(-\infty, 0]$.
6. Describes that as x increases toward 0 from the left ($x < 0$), the function values y increase for both functions.

Table 7: Example of math pick points.

of model, with a per-device batch size of 4 and gradient accumulation over 2 steps. Following the LoRA+ setting, we use a learning-rate ratio of 16.0 for LoRA parameters. For both settings, we employ the AdamW optimiser with a cosine learning-rate scheduler, an initial learning rate of 5×10^{-5} , a warmup ratio of 0.1, and gradient clipping with a maximum gradient norm of 1.0. All models are trained for 2 epochs using bfloat16 precision. To support long interleaved math-code reasoning trajectories, the maximum sequence length is set to 100k tokens. All experiments are conducted on 8 NVIDIA A800-SXM4-80GB GPUs. For the classifier, we use sklearn to implement them using default hyper-parameters.

Prompts. The prompts used for evaluating textual reasoning correctness (Text), code correctness (Code), text-code consistency (Text-Code), final answer accuracy (Ans Acc), and rule extraction are provided in Table 8, Table 11, Table 12, and Table 13, respectively.

A.2 Human Evaluation Protocol

To validate the reliability of the LLM-based automatic scoring pipeline, we conduct a human evaluation on a randomly sampled subset of GeoMath-Code. The goal is to assess whether automatic scores are consistent with expert judgments on textual reasoning correctness, code-generated diagram correctness, and text-code consistency.

Sample selection. We sample 100 examples from the test set, stratified by geometry topic and question type. Each example contains the original problem, the reference answer, the generated multi-step solution, the generated Python code for each reasoning step, and the rendered diagram. The automatic LLM scores are hidden from annotators

during evaluation.

Annotators. Each sample is evaluated by one PhD-level annotator with mathematical or geometry problem-solving background. Annotator is instructed to focus on mathematical correctness rather than stylistic quality.

Evaluation dimensions. Annotator scores each sample along three dimensions:

1. Textual reasoning correctness. Whether the generated reasoning follows valid mathematical logic, uses appropriate geometric facts, and reaches intermediate conclusions correctly.

2. Final answer correctness. Whether the final answer is equivalent to the reference answer, allowing equivalent expressions, reordered items, or semantically identical explanations.

3. Diagram correctness. Whether the Python diagram correctly include the mathematical objects, including equations, points, angles, curves, annotations, auxiliary constructions, and plotting ranges.

Scoring rubric. Each dimension is scored on a 0–5 scale:

- **5:** Fully correct; no mathematical or consistency errors.
- **4:** Mostly correct; only minor omissions or harmless presentation issues.
- **3:** Partially correct; contains noticeable errors but preserves the main reasoning direction.
- **2:** Major errors; reasoning, code, or diagram is substantially flawed.
- **1:** Mostly incorrect; only minimal relevant content is correct.
- **0:** Missing, invalid, irrelevant, or completely incorrect.

Annotation guidelines. Annotator is asked to apply the following rules:

- Accept mathematically equivalent reasoning even if it differs from the reference solution.
- Do not require theorem names if the theorem is correctly applied.
- Penalize unsupported conclusions, incorrect theorem use, missing key geometric conditions, or invalid algebraic manipulation.

You are a geometry auto-marker.

Input:

* problem
 * student_solution
 * reference_dict=
 "overall_strategy", "key_pick_points", "rules"

Task:

Mark the student solution against the reference_dict.

Rules:

* Accept equivalent valid reasoning
 * Accept different order of steps
 * Accept implicit theorem use if clearly applied
 * Do not require theorem names
 * Do not award full credit for unsupported conclusions
 * Penalize theorem misuse, missing essential checkpoints, and logical gaps
 * Base marks mainly on key_pick_points

Scoring rules:

- 5 = fully correct
 - 4 = minor issue, overall mathematically correct
 - 3 = partially correct, noticeable error
 - 2 = major error
 - 1 = mostly incorrect
 - 0 = completely incorrect or missing

Return STRICT JSON only:

- "overall_strategy_assessment": 0-5,
 - "pick_point_assessment": 0-5,
 - "rule_assessment": 0-5,

Table 8: Example of the prompt used for textual reasoning evaluation. The final Text score is computed as the average of the pick_point_assessment and rule_assessment scores.

MLLM	Opt.	Ans Acc	Text	Code Acc	Code	Text Code	Avg.
Qwen3-VL-Ins-8B	-	0.33	0.38	0.59	0.47	0.41	0.44
Qwen3-VL-Ins-8B	SFT	0.49	0.60	0.97	0.80	0.67	0.71
Qwen3-VL-Think-8B	SFT	0.45	0.52	0.87	0.72	0.61	0.63
Qwen3-VL-Ins-8B	LoRA	0.42	0.53	0.86	0.70	0.58	0.62
Qwen3.5-4B	SFT	0.44	0.53	0.94	0.75	0.62	0.66
Qwen3.5-9B	SFT	0.56	0.65	0.97	0.84	0.73	0.75
Qwen3.5-9B	LoRA	0.57	0.65	0.94	0.82	0.72	0.74
LLaVA-NEXT-8B	-	0.00	0.00	0.00	0.00	0.00	0.00
LLaVA-NEXT-8B	SFT	0.16	0.25	0.85	0.45	0.28	0.40
InternVL3.5-8B	-	0.30	0.35	0.54	0.60	0.50	0.46
InternVL3.5-8B	SFT	0.49	0.61	0.96	0.79	0.67	0.70

Table 9: GPT-5.1 evaluation results.

- For code evaluation, focus on mathematical validity rather than visual aesthetics.
- A rendered diagram should be considered correct if it faithfully represents the required geometric or functional relationship, even if its style differs from the reference.

Pass/fail conversion. For consistency with the automatic filtering pipeline, we additionally convert human scores into binary labels: scores ≥ 3 are treated as passing, while scores < 3 are treated as failing. We then report agreement between human pass/fail labels and LLM-based pass/fail decisions.

Table 14 reports the Spearman correlation be-

MLLM	Opt.	Ans Acc	Text	Code Acc	Code	Text Code	Avg.
Qwen3-VL-Ins-8B	-	0.30	0.36	0.58	0.39	0.35	0.39
Qwen3-VL-Ins-8B	SFT	0.46	0.55	0.97	0.68	0.66	0.69
Qwen3-VL-Think-8B	SFT	0.42	0.48	0.85	0.66	0.57	0.60
Qwen3-VL-Ins-8B	LoRA	0.39	0.49	0.84	0.65	0.55	0.58
Qwen3.5-4B	SFT	0.40	0.49	0.92	0.71	0.58	0.62
Qwen3.5-9B	SFT	0.55	0.64	0.97	0.69	0.69	0.71
Qwen3.5-9B	LoRA	0.52	0.62	0.93	0.77	0.67	0.70
LLaVA-NEXT-8B	-	0.00	0.00	0.00	0.00	0.00	0.00
LLaVA-NEXT-8B	SFT	0.13	0.21	0.81	0.41	0.24	0.36
InternVL3.5-8B	-	0.27	0.31	0.51	0.54	0.44	0.41
InternVL3.5-8B	SFT	0.46	0.56	0.96	0.68	0.66	0.66

Table 10: DeepSeek-V4-Flash evaluation results.

<p>You are a Python code auto-marker for geometry/math visualization tasks.</p> <p>Input:</p> <ul style="list-style-type: none"> - the GeoMath problem - the multi-step solution - the Python code used to generate the image for each step <p>Task:</p> <p>Verify whether the code is mathematically correct.</p> <p>Score each category from 0 to 5:</p> <ul style="list-style-type: none"> - equation: whether the implemented functions exactly match the problem equations - properties: whether key properties derived from the formulas are correct, such as vertex, axis of symmetry, and opening direction, etc. - points: whether sample points used or implied by the code agree with the true function values - range: whether the plotting range is appropriate - annotations: whether labels, arrows, symmetry lines, marked vertices, and other annotations are mathematically consistent with the plotted functions - consistency: whether the textual reasoning step and the corresponding code are consistent with each other <p>Scoring rules:</p> <ul style="list-style-type: none"> - 5 = fully correct - 4 = minor issue, overall mathematically correct - 3 = partially correct, noticeable error - 2 = major error - 1 = mostly incorrect - 0 = completely incorrect or missing <p>Return strict JSON with fields:</p> <ul style="list-style-type: none"> - "equation": 0-5, - "properties": 0-5, - "points": 0-5, - "range": 0-5, - "annotations": 0-5, - "consistency": 0-5
--

Table 11: Example of the prompt used for code correctness evaluation. The final Code score is computed as the average of the equation, properties, points, range, and annotations scores, while the Text-Code score corresponds to the consistency score.

tween LLM evaluators and human evaluators. We observe a particularly high correlation when using Gemini3-Pro, indicating strong agreement with

human judgments. For diagram evaluation, the majority of generated diagrams satisfy the required mathematical and structural constraints.

You are a strict grading assistant.
 Given a question, a ground truth answer, and a predicted answer, decide if the predicted answer is semantically correct.
 Rules:
 - Focus only on correctness relative to the ground truth.
 - Ignore style, wording, and extra explanation.

Finally, you should output **correct** or **incorrect** ONLY.
 Return strict JSON with fields:
 - "ans_match": correct/incorrect

Table 12: Example of the prompt used for final answer evaluation. This prompt is only used for marking short-description question-answer pairs.

Extract the reasoning structure and pick points from this geometry math solution.

Given:

A geometry problem
 A multi-step solution

Produce:

- overall strategy
- key pick points used for marking the solution
- theorem/rule used at each step

Return strict JSON with fields:

- overall_strategy: "...",
- key_pick_points: ["...", ...],
- rules: [step, rule, rule_type, explicit_or_implicit],

Additional constraints:

- Rules MUST be universal (not problem-specific wording)
- Rules MUST be symbolic whenever possible
- If symbolic form is not possible, use minimal canonical phrasing
- Do NOT include explanations, only abstractions of rules

Table 13: Example of the prompt used for extracting symbolic mathematical rules and reasoning pick-points from multi-step geometry solutions.

Evaluator 1	Evaluator 2	Spearman
Human	Gemini3-Pro	0.90
Human	DeepSeek-V4-Flash	0.82
Human	GPT-5.1	0.61

Table 14: Spearman correlation between human evaluators and LLM evaluators on the textual reasoning correctness.

Purpose. This human evaluation is used only to validate the reliability of the automatic scoring pipeline, not to replace the full-scale automatic evaluation. In particular, it verifies whether LLM-based judgments align with expert human assessments on reasoning correctness, code correctness, and text-code consistency.

A.3 Additional Results

Table 16 and 17 display the Pearson and Spearman correlation from GPT-5.1 and DeepSeek-V4-Flash, respectively. We can observe that incorporating pick-point and rule-based instruction during evaluation can improve the correlation between Ans Acc and Text.

Table 3 displays the Spearman correlation between different LLM evaluators. We observe that the correlation between Gemini3-Pro and DeepSeek-V4-Flash is consistently higher than their correlations with GPT-5.1, indicating that Gemini3-Pro and DeepSeek-V4-Flash exhibit more aligned evaluation behaviours for intermediate reasoning assessment.

Model	Algebra	Analytic	Cal.	Trig.	Plane	Solid	Stats.	Trans.	Avg.
GPT5.1	0.60	0.60	0.66	0.68	0.42	0.42	0.68	0.38	0.55
GPT5.2	0.60	0.62	0.80	0.74	0.50	0.48	0.84	0.40	0.62
Gemini3 Pro	0.70	0.70	0.82	0.84	0.68	0.60	0.84	0.66	0.73
Gemini3 Flash	0.70	0.72	0.84	0.84	0.64	0.62	0.76	0.72	0.73

Table 15: Chosen of pipeline generator, 100 samples of each category randomly sampled from MathCanvas corpus.

MLLM	Ans	Acc-Text	Ans	Acc-Text Code
<i>without rule instruction</i>				
Qwen3-VL-Ins-8B-SFT	0.43	0.43	0.36	0.37
Qwen3.5-9B-SFT	0.46	0.47	0.37	0.38
Qwen3.5-9B-LoRA	0.47	0.47	0.30	0.29
InternVL3.5-8B-SFT	0.50	0.49	0.39	0.40
<i>with rule instruction</i>				
Qwen3-VL-Ins-8B-SFT	0.61	0.59	0.36	0.36
Qwen3.5-9B-SFT	0.62	0.62	0.34	0.35
Qwen3.5-9B-LoRA	0.64	0.63	0.30	0.30
InternVL3.5-8B-SFT	0.64	0.61	0.37	0.38

Table 16: GPT-5.1: Pearson (left) and Spearman (right) correlation between different metrics.

MLLM	Ans	Acc-Text	Ans	Acc-Text Code
<i>without rule instruction</i>				
Qwen3-VL-Ins-8B-SFT	0.48	0.47	0.22	0.24
Qwen3.5-9B-SFT	0.49	0.48	0.22	0.23
Qwen3.5-9B-LoRA	0.49	0.48	0.21	0.22
InternVL3.5-8B-SFT	0.47	0.48	0.24	0.22
<i>with rule instruction</i>				
Qwen3-VL-Ins-8B-SFT	0.68	0.68	0.22	0.23
Qwen3.5-9B-SFT	0.68	0.67	0.23	0.23
Qwen3.5-9B-LoRA	0.69	0.68	0.24	0.23
InternVL3.5-8B-SFT	0.69	0.68	0.22	0.23

Table 17: DeepSeek-V4-Flash: Pearson (left) and Spearman (right) correlation between different metrics.

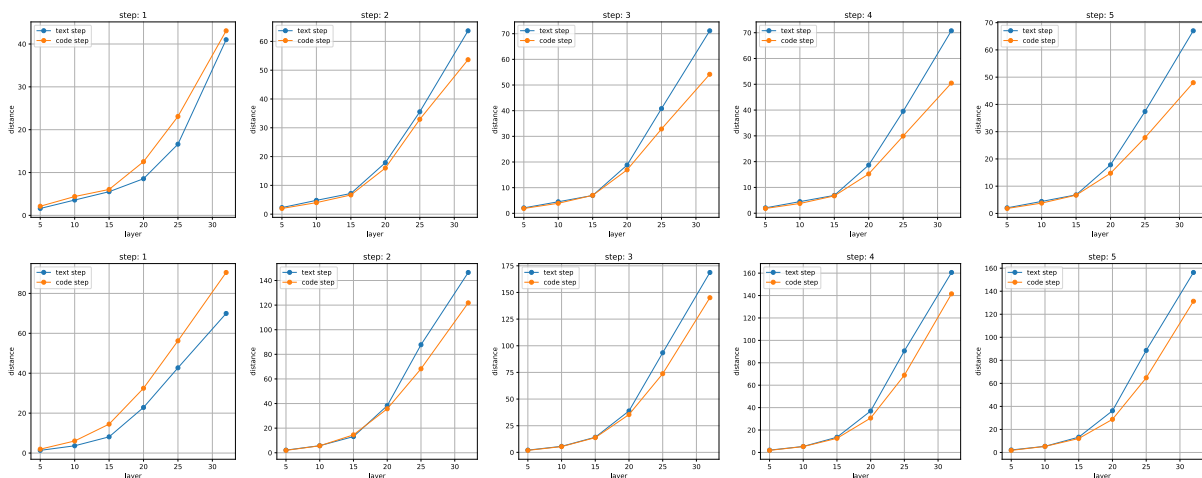


Figure 6: Average euclidean distance of different steps at different layers (Top: Qwen3-ins-8B, bottom: Qwen3-ins-8B-SFT).

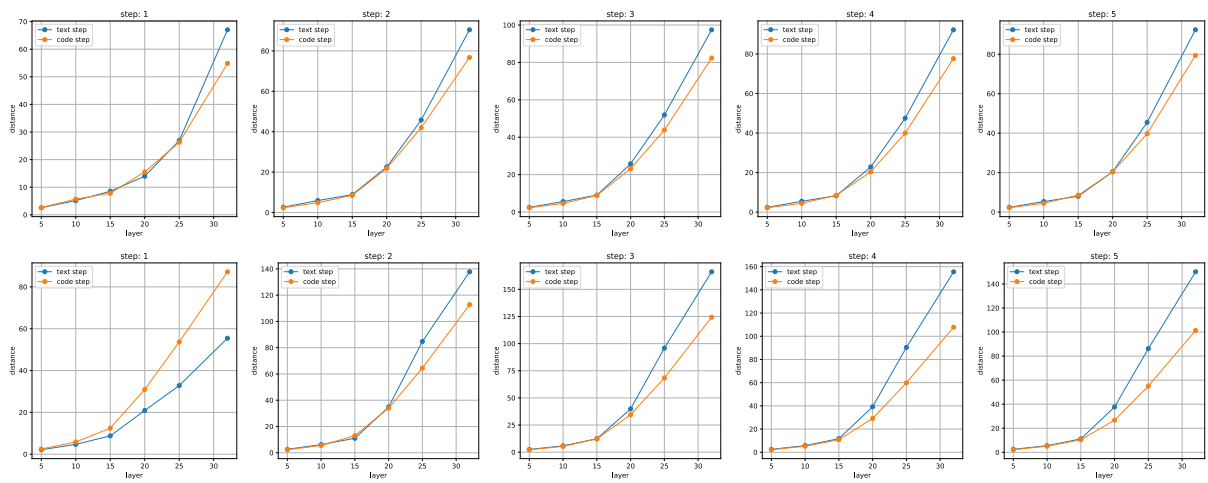


Figure 7: Average euclidean distance of different steps at different layers (Top: InternVL3.5-8B, bottom: InternVL3.5-8B-SFT).